AGU PUBLICATIONS

Water Resources Research

RESEARCH ARTICLE
10.1002/2013WR014132

Key Points:
- A high-resolution hydrological model of the Black Sea Basin is built
- We included river discharge, crop yield, and nitrate load in calibration
- Blue and green water resources of the Basin are calculated at subbasin level

Correspondence to:
E. Rouholahnejad,
elham.rouholahnejad@eawag.ch

Citation:
Rouholahnejad, E., K. C. Abbaspour, R. Srinivasan, V. Bacu, and A. Lehmann (2014), Water resources of the Black Sea Basin at high spatial and temporal resolution, *Water Resour. Res.*, *50*, 5866–5885, doi:10.1002/2013WR014132.

Received 16 MAY 2013
Accepted 24 JUN 2014
Accepted article online 30 JUN 2014
Published online 16 JUL 2014
Corrected 5 AUG 2014

This article was corrected on 5 AUG 2014. See the end of the full text for details.

Water resources of the Black Sea Basin at high spatial and temporal resolution

Elham Rouholahnejad[1,2], Karim C. Abbaspour[1], Raghvan Srinivasan[3], Victor Bacu[4], and Anthony Lehmann[5]

[1]Eawag, Swiss Federal Institute of Aquatic Science and Technology, Duebendorf, Switzerland, [2]ETH Zürich, Institute of Terrestrial Ecosystem, Zurich, Switzerland, [3]Texas A&M University, Texas Agricultural Experimental Station, Spatial Science Laboratory, College Station, Texas, USA, [4]Department of Computer Science, Technical University of Cluj-Napoca, Cluj-Napoca, Romania, [5]Climatic Change and Climate Impacts, University of Geneva, Carouge, Switzerland

Abstract The pressure on water resources, deteriorating water quality, and uncertainties associated with the climate change create an environment of conflict in large and complex river system. The Black Sea Basin (BSB), in particular, suffers from ecological unsustainability and inadequate resource management leading to severe environmental, social, and economical problems. To better tackle the future challenges, we used the Soil and Water Assessment Tool (SWAT) to model the hydrology of the BSB coupling water quantity, water quality, and crop yield components. The hydrological model of the BSB was calibrated and validated considering sensitivity and uncertainty analysis. River discharges, nitrate loads, and crop yields were used to calibrate the model. Employing grid technology improved calibration computation time by more than an order of magnitude. We calculated components of water resources such as river discharge, infiltration, aquifer recharge, soil moisture, and actual and potential evapotranspiration. Furthermore, available water resources were calculated at subbasin spatial and monthly temporal levels. Within this framework, a comprehensive database of the BSB was created to fill the existing gaps in water resources data in the region. In this paper, we discuss the challenges of building a large-scale model in fine spatial and temporal detail. This study provides the basis for further research on the impacts of climate and land use change on water resources in the BSB.

1. Introduction

The pressures on water resources and increasing conflict of interest present a huge water management challenge in the Black Sea Basin (BSB) [*Global International Waters Assessment* (*GIWA*), 2005]. The small-scale sectoral structure of water management is now reaching its limits. The integrated management of water in the Basin requires a new level of consideration where water bodies are to be viewed in the context of the whole river system and managed as a unit within their basins. This is of key interest for efficient and targeted water management through regional coordination, transparent balancing of interests, and clear priority setting [*Water Agenda 21*, 2011]. A frequently advocated approach is to have adequate knowledge of temporal and spatial variability of the fresh water availability and water quality [*United Nations Environment Program* (*UNEP*), 2006].

The BSB is internationally recognized for its ecologically unsustainable development and inadequate resource management leading to severe environmental, social, and economical problems. In 1995, it was rated as being of the highest concern in five out of seven environmental categories, making it the worst of any of the European seas [*Stanners and Boudreau*, 1995]. In another study, the German Advisory Council on Global Change (WBGU) states that the Black Sea is likely to experience (i) a degradation of freshwater resources; (ii) an increase of storm and flood disasters; (iii) a decline in food production; and (iv) environmentally induced migration [*Wissenschaftlicher Beirat Globale Umweltveränderung* (*WBGU*), 2007]. In addition, transboundary pollution effects (TPE) can be seen with respect to all economic sectors. Transboundary pollution is the pollution that originates in one country but causes damage in another country's environment, by crossing borders in the rivers [*Paleari*, 2005].

Furthermore, the Intergovernmental Panel on Climate Change [*IPCC*, 2007] predicts important changes in the coming decades that will not only modify climate patterns in terms of temperature and rainfall, but will

also drastically change freshwater resources qualitatively and quantitatively. This is expected to lead to more floods or droughts in different regions, lowering of drinking water quality, increased risk of water-borne diseases, and irrigation problems. These changes may trigger socio-economic crises that need to be addressed well in advance of the events in order to reduce the associated risks.

Previous research, which addressed water quantity and water quality in the BSB, includes a few global and regional studies. WaterGAP2 [*Alcamo et al*., 2003; *Döll et al*., 2003] is a global model for water availability and water use. This model focuses on the global hydrology at grid scale (30 arc min) considering 3565 major basins in the world with the drainage areas greater than 2500 km^2. The model was initially used to estimate the water availability and demand and provides relatively limited water cycle-related components. In WaterGAP3 [*Aus der Beek et al*., 2012], a regional version of WaterGAP2, the hydrological fluxes draining into Mediterranean and Black Sea were modeled with improved spatial resolution (5 arc min), snow melt, and water use. However, results using WaterGAP3 and WaterGAP2 are not significantly different in the BSB [*Aus der Beek et al*., 2012]. In a different approach, *Meigh et al*. [1999] developed a grid-based model Global Water Availability Assessment (GWAVA) to predict water resources scarcity at continental and global scales. This model has recently been further developed to include water quality [*Dumont et al*., 2012]. Using a statistical approach, *Grizzetti et al*. [2008] assessed nitrogen content of surface water for major European river basins. Furthermore, discharges of water and nutrient to the Mediterranean and Black Sea are reported in a study by *Ludwig et al*. [2009] for major rivers.

Next to the above mentioned studies, there are a few other investigations on the status of river basins in the BSB [*Sukhodolov et al*., 2009; *Sommerwerk et al*., 2009; *Wolfram and Bach*, 2009]. However, often average loads entering the Sea are reported without adequate spatial and temporal resolution on the current and future freshwater availability for the entire BSB. General shortcomings of the previous studies are missing detail information on model inputs and outputs, unavailability of their input data, coarse spatial resolution and scale of the models, and missing model calibration/validation and uncertainty analysis components.

In recent years, improvements in integrated hydrological modeling, advancements in calibration and uncertainty analysis tools, and availability of grid technology for model execution allow building more detailed and holistic models. These models account for processes such as water quantity and quality, soil, climate, land use, agricultural managements, and nutrient cycling in a coupled single package. The aim of the project is to build a high-resolution model of the entire BSB and to look at the impact of land use and climate change on the water resources. The reason for building a single model of the BSB is to have a uniformly calibrated model of the region rather than several disparately calibrated models. A high-resolution large-scale model has the advantages of allowing a holistic look at the Basin while retaining the small-scale system variabilities. The objectives of the current study are to: (i) gather and share a comprehensive database of the BSB, (ii) model the hydrology of the entire BSB by including agricultural management and crop yield to better quantify water quantity and water quality at daily time step and subbasin level, (iii) calibrate and validate the model with uncertainty analysis using grid technology, (iv) produce a relatively accurate picture of water resources availability, reliability, and pressures in the Basin.

To achieve the objectives of this research, we used the program Soil and Water Assessment Tool (SWAT) [*Arnold et al*., 1998]. SWAT was used because it is a continuous time and spatially distributed watershed model, in which hydrological processes and water quality are coupled with crop growth and agricultural management practices. The program was successfully applied in a wide range of scales and environmental conditions [*Gassman et al*., 2007]. Another advantage of SWAT is its modular implementation where different processes can be selected.

For calibration and uncertainty analysis in this study, we used the Sequential Uncertainty Fitting program SUFI-2 [*Abbaspour et al*., 2004, 2007]. SUFI-2 is a tool for sensitivity analysis, multisite calibration, and uncertainty analysis. It lends itself easily to parallelization and is capable of analyzing a large number of parameters and measured data from many gauging stations (outlets) simultaneously. SUFI-2 is linked to SWAT in the SWAT-CUP software [*Abbaspour*, 2011]. *Yang et al*. [2008] found that SUFI-2 needed the smallest number of model runs to achieve a similarly good calibration and prediction uncertainty results in comparison with four other techniques. This efficiency is of great importance when dealing with computationally intensive, complex large-scale models. We ran parallelized SUFI-2 on grid system described by *Rouholahnejad et al*. [2012] and *Gorgan et al*. [2012].

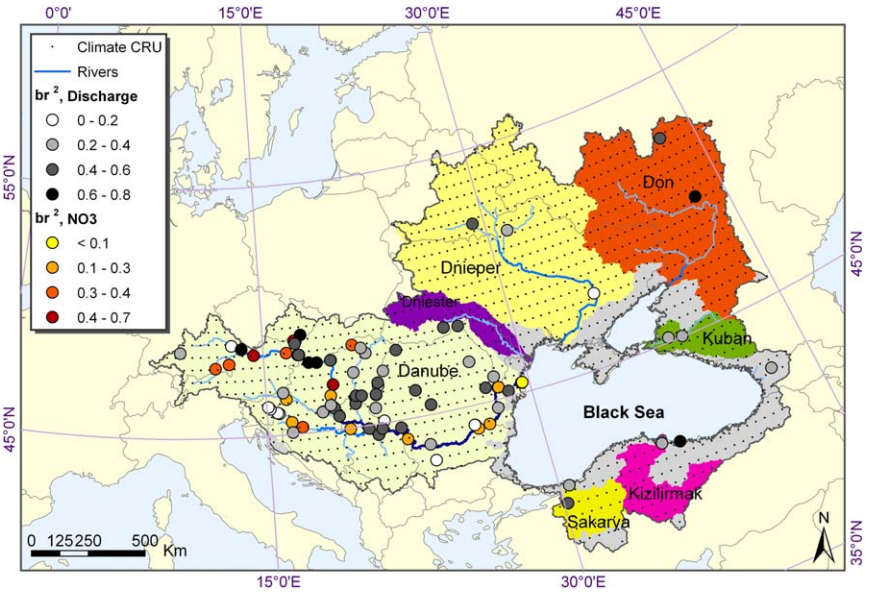

Figure 1. Illustration of Black Sea Basin showing major rivers and measured stations of climate, discharge, and nitrate. Also shown is the comparison of observed and simulated discharge and nitrate using the efficiency criterion bR^2. The six large river basins of Danube, Dnieper, Don, Kuban, Kizilirmak, and Sakarya are highlighted.

2. Material and Methods

2.1. Study Area

The Black Sea Basin (Figure 1) with a total area of 2.3×10^6 km^2 drains rivers of 23 European and Asian countries (Austria, Belarus, Bosnia, Bulgaria, Croatia, Czech Republic, Georgia, Germany, Hungary, Moldova, Montenegro, Romania, Russia, Serbia, Slovakia, Slovenia, Turkey, Ukraine, Italy, Switzerland, Poland, Albania, and Macedonia) to the Black Sea. The Basin is inhabited by a total population of around 160 million people [*Black Sea Investment Facility (BSEI)*, 2005]. It is mountainous in the east and south, in the Caucasus, and in Anatolia, and to the northwest with the Carpathians in the Ukraine and Romania. Most of the rest of the Black Sea's western and northern neighborhood is low lying. Mean annual air temperature shows a distinct north-south gradient from <-3°C to >15°C. The precipitation pattern is characterized by a west-east gradient from a high of >3000 mm yr^{-1} to a low of <190 mm yr^{-1} [*Tockner et al*., 2009]. The dominant land use in the basin is agricultural with 65% of coverage according to MODIS Land Cover [*NASA*, 2001]. Major rivers draining into the Black Sea include Danube, Dnieper, and Don. The greatest sources of diffuse pollution are agricultural and households not connected to sewer systems [*European Environmental Agency (EEA)*, 2010].

2.2. Soil Water Assessment Tool (SWAT)

SWAT was used to simulate hydrology, water quality, and vegetation growth in BSB. SWAT is a process-based, semidistributed, hydrologic model. The model has been developed to quantify the impact of land management practices on water, sediment, and agricultural chemical yields in large complex watersheds with varying soils, land uses, and management conditions over long periods of time. SWAT was chosen because of the close linkage between its development purposes and the objectives of this project, open access to the source code, and its successful application in a wide range of scales and environmental conditions.

The main components of SWAT are hydrology, climate, nutrient cycling, soil temperature, sediment movement, crop growth, agricultural management, and pesticide dynamics. SWAT is a continuous simulation model operating on a daily time step. The spatial heterogeneity of the watershed is preserved by topographically dividing the basin into multiple subbasins. These are further subdivided into hydrologic response units (HRU) based on soil, land use, and slope characteristics. These subdivisions enable the model to reflect differences in evapotranspiration for various crops and soils. In each HRU and on each time step, the hydrologic and vegetation-growth processes are simulated based on the curve number rainfall-runoff partitioning and the heat unit phenological development method [*Neitsch et al*., 2009].

Runoff is predicted separately for each HRU and routed to obtain the total model runoff for the watershed. The routing phase of the hydrologic cycle in SWAT is the movement of water, nitrate, etc., through the channel network of the watershed. Once SWAT determines the loadings of water, sediment, nutrients, and pesticides to the main channel, the loadings are routed through the stream network of the watershed. In addition to keeping track of mass flow in the channel, SWAT models the transformation of chemicals in the stream and streambed.

Energy availability governs vegetation phenology. At each point in the growth cycle, biomass production is derived from the interception of solar radiation by leaves, plant-specific radiation use efficiency, and leaf area index (LAI). Crop yield is calculated at harvest by multiplying the above-ground biomass with the harvest index. The harvest index is a fraction of the above-ground plant dry biomass removed as dry yield. Plant growth is limited by temperature, water, and nutrient availability in the soil and is influenced by agricultural management (e.g., fertilization, irrigation, and timing of operations). A detailed description of SWAT's theory can be obtained in *Neitsch et al*. [2009].

2.3. Input Data and Model Outputs

BSB Digital Elevation Model (DEM) at 90 m spatial resolution was extracted from SRTM [*Jarvis et al*., 2008]. The river network data set was from European Catchments and Rivers Network System [*EEA Catchments and Rivers Network System (ECRINS) v1.1*, 2012]. The ECRINS river map was corrected in the areas where there was a mismatch with DEM to achieve a correct flow direction.

The soil data were obtained from the FAO-UNESCO global soil map [*Food and Agricultural Organization (FAO)*, 1995], which provides data for 5000 soil types comprising two layers (0–30 cm and 30–100 cm depth) at a spatial resolution of 5 km.

Four different land uses were available for the region: (i) Global Land Cover Characterization (GLCC) at 1 km spatial resolution [*U. S. Geological Survey (USGS)*, 2008], (ii) MODIS land cover with spatial resolution of 500 m [*NASA*, 2001], (iii) GlobCover with spatial resolution of 300 m [*Environmental Space Agency (ESA)*, 2008], (iv) Global Corine at 300 m spatial resolution [*Environmental Space Agency (ESA)*, 2010].

Two different climate databases were available: measured and gridded data. Measured climate included 456 rainfall and 678 temperature stations mainly collected from National Climatic Data Centre (NCDC; http://www.climate.gov/#dataServices/dataLibrary), the European Climate Assessment and Dataset (ECAD) [*Haylock et al*., 2008], Turkish Ministry of Forest and Water Affairs (MEF), and Romanian National Institute of Hydrology and Water Management (INHGA) for the period of 1970–2008. Only stations with $<$20% missing data were included in the model. Gridded data are constructed from measured climate stations and interpolated to grid resolution. We used data from Climate Research Units [*Climatic Research Unit (CRU)*, 2008; *Mitchell and Jones*, 2005] at 0.5° resolution amounting to 1147 grid points. The daily global solar radiation data were obtained from 6110 virtual stations at 0.5° resolution for the duration of 1960–2001 [*Weedon et al*., 2011].

Monthly river discharge data for model calibration and validation were obtained from Global Runoff Data Center [*Global Runoff Data Centre (GRDC)*, 2011], National Institute of Hydrology and Water Management (INHGA) and Danube Delta National Institute for Research and Development (DDNI) in Romania, and Turkish Ministry of Forest and Water Affairs (MEF) for the period 1970–2008. Only stations with $<$20% missing data and minimum length of 5 years were included in calibration-validation process. This led to 144 discharge outlets where 37 of them also contained nitrate data from International Commission for the Protection of the Danube River (ICPDR). These outlets had differing beginning and ending time periods.

Point sources were also assigned to each subbasin in the model. The nutrient loads of subbasins were calculated based on the population of the subbasins, the percentage of population connected to wastewater treatment plant, and the average rate of nitrogen per population equivalent. Population percentage connected to any kind of sewage treatment was derived from Eurostat for the period of 2000–2009. This share was above 80% in approximately half of the European Union countries for which data are available, rising to 95% in Germany. At the other end, less than one in two households were connected to urban wastewater treatment in Bulgaria and Romania. In terms of treatment levels, tertiary wastewater treatment was most common in Germany, Austria, and Italy where at least four in every five persons were connected to this type of wastewater treatment. In contrast, no more than 1% of the population was connected to tertiary

wastewater treatment in Romania and Bulgaria. We assumed the treatment efficiency to be 80% in all countries with 20% loading directly into surface waters and hence considered as point sources.

To account for industrial and household releases, *Zessner and Lindtner* [2005] calculated the nitrogen load to be 8.8 g N P_e^{-1} d^{-1}, where P_e is population equivalent, which is the number expressing the ratio of the sum of the pollution load produced during 24 h by industrial facilities and household to the individual pollution load in household sewage produced by one person in the same time. The ratio of population and P_e varies in a way that 80% of the treatment plants lie in the range of 0.4–0.9. The average value of this ratio is assumed to be 0.63 [*Zessner and Lindtner*, 2005]. The nutrient load is calculated as

$$L_N = P_e I_N [(1 - S_{rate}) + (1 - T_{eff}) S_{rate}] \quad (1)$$

where L_N is the nitrogen load entering rivers in subbasins (g d^{-1}), T_{eff} is the wastewater treatment efficiency, I_N is the average input of nitrogen from household to wastewater (g N P_e^{-1} d^{-1}), and S_{rate} is the percentage of the population connected to any kind of sewage treatment. We used population map of year 2005 from the Center for International Earth Science Information Network in 2.5 arc min resolution [*Center for International Earth Science Information Network (CIESIN)*, 2005] and extrapolated to other years based on the national population growth rate provided by the World Bank.

Cropping area and the start and end month of cropping periods in the BSB countries were derived from MIRCA2000 database on global monthly irrigated and rain-fed cropping areas around the year 2000 (5 year average), at a spatial resolution of 5 arc min [*Portmann et al*., 2010]. This database represents multicropping systems and maximizes consistency with census-based national and subnational statistics. Crop yield data were obtained from McGill University [*Monfreda et al*., 2008] at 5 min resolution. This data were 5 year averages around the year 2000 and were used to calculate per subbasin crop yields for maize, barley, and wheat. Country-based crop yield was obtained from FAOSTAT database [*Food and Agricultural Organization Statistics (FAOSTAT)*, 2013].

SWAT produces a large amount of output variables. In this study we look at the water cycle components, crop yield, and nitrate concentration in rivers. Using the water cycle constituents calculated in SWAT, we could also calculate water resources components such as "blue water," "green water flow," and "green water storage." Currently, the definition of blue water is generally accepted as the sum of the river discharge and the deep groundwater recharge. This is in essence the water resources by the traditional hydrological and engineering definition. There exist slightly different definitions for the term green water. *Falkenmark and Rockstrom* [2006] differentiate between the green water "resource" and the green water "flow." According to their definition, green water resource is the moisture in the soil, which is a renewable resource and can potentially generate economic returns, as it is the source for rain-fed agriculture. The green water flow is composed of the actual evaporation (the nonproductive part) and the actual transpiration (the productive part), commonly referred to together as the actual evapotranspiration.

2.4. Model Setup

The subbasins were delineated with a threshold area of 100 km^2 yielding 12,982 subbasin. This was the smallest threshold that could be used to build the ArcSWAT project on a 64 bit laptop with 2.7 GHz processors, 4 cores, 8 GB of RAM, and Windows7 operating system. This is because of memory limitation and inefficiency of ArcGIS in handling large raster calculation. In addition, the personal geodatabase of ArcSWAT created by ArcGIS9 has a limitation of 2 GB on the file size. Fourteen different land cover classes of MODIS were assigned to land uses in the SWAT database. Subsequently, each of the 12,982 subbasins was spilt into unique combinations of slope, land use classes, and soil types resulting in 89,202 Hydrologic Response Unit (HRU). Three classes of slope (0–3%, 3–6%, and >6%) were used in the subbasin discretization. We also used five elevation bands in each subbasin to adjust for orographic change in temperature ($-6^{\circ}C$ km^{-1}) and precipitation (670 mm km^{-1}) after some initial fitting.

Twenty-five different management plans were designed based on the crop types, cropping dates, winter or summer crops, irrigated or rain-fed applications. Each HRU then corresponded to a management plan. Exclusive agricultural classes were assigned to each country so that desired management could be defined at the national level. Subsequently, agricultural areas within these classes were subdivided proportional to the cropping areas of irrigated/rain-fed, winter/spring types for wheat, maize, and barely. The three major

crops were allocated to agricultural lands in MODIS proportional to their contribution in each country's harvested areas as reported by MIRACA2000 [*Portmann et al*., 2010].

The option of automatic fertilization in SWAT was employed to meet crop need and the annual maximum application amount was set to 300 kg N ha^{-1}. This assumption leads to underestimation of nitrogen in areas where application is more than crop need. Elemental nitrogen and elemental phosphors were applied to the agricultural lands in each subbasin as the main fertilizer in BSB. An additional nitrogen input of 1.2 mg N l^{-1} was assumed in the rainfall. It is notable that in the MODIS classification agricultural land does not include permanent grassland.

We invoked automatic irrigation based on plant water demand in such a way as to minimize crop water stress in irrigated lands. In this study, potential evapotranspiration (PET) was estimated using the Hargreaves method [*Hargreaves et al*., 1985] while actual evapotranspiration (ET) was estimated based on *Ritchie* [1972].

The simulation period was 1970–2006 using 3 years of initialization (1970–1972) as warm up period. As each station had a different beginning and ending time periods, the model was calibrated from 1973 to 1996 and validated from 1997 to 2006 for discharge, and because of fewer data in the early years, the nitrate loads were calibrated from 1973 to 2000 and validated from 2001 to 2006. Within these general years different stations had different data availability periods. Given the disparity in data lengths and timing, this was the most sensible division of data between calibration and validation time period. SWAT always runs on daily time step, but we used monthly outputs for calibration and validation of the model. Using SWAT 2009, it took 42 h for a single-model run on the laptop where ArcSWAT project was built.

2.5. Model Calibration Procedure

Sensitivity, calibration, validation, and uncertainty analysis were performed for water quantity, water quality, and crop yield using river discharges, nitrate loads in rivers, and yields of wheat, barley, and maize. SUFI-2 was used for calibration and uncertainty analysis. In SUFI-2, all sources of uncertainties are mapped to a set of parameter ranges. They are calibrated with the dual aim of bracketing most of the observed data with as narrow as possible uncertainty band. Initially, a set of meaningful parameter ranges are assigned to calibrating parameters based on literature, knowledge of site processes, and sensitivity analyses. Then a set of Latin hypercube samples are drawn from the parameter ranges, and the objective function is calculated for each parameter set. The uncertainty is quantified at the 2.5% and 97.5% levels of the cumulative frequency distribution of all simulated output values, and it is referred to as the 95% prediction uncertainty (95PPU). The lower, middle, and upper boundaries of the 95PPU (L95PPU, M95PPU, and U95PPU) reflect the 2.5, 50, and 97.5 percentiles of the distribution, respectively. Values at the 50% probability level are used for drawing average long-term maps of different variables. The goodness of model performance in terms of calibration and uncertainty level is evaluated using the *P-factor* and the *R-factor* indices. The *P-factor* is the percentage of measured data bracketed by the 95PPU band. It ranges from 0 to 1 where 1 is ideal and means all of the measured data are within the uncertainty band (i.e., model prediction). The *R-factor* is the average width of the band divided by the standard deviation of the measured variable. It ranges from 0 to ∞ where 0 reflects a perfect match with the observation. Based on the experience, an *R-factor* of around 1 is usually desirable [*Abbaspour et al*., 2007] where the thickness of the uncertainty band does not exceed the measured standard deviation. SUFI-2 allows for a measurement error of about 10% to be assigned to all observed variables, which are accounted for in the 95PPU calculations.

Coefficient of determination r^2 is a measure of dispersion around the mean of the observed and predicted values and can be used as an efficiency criteria. The range of r^2 lies between 0 and 1 which describes how much of the observed dispersion is explained by the prediction. A value of zero means no correlation at all whereas a value of 1 means that the dispersion of the prediction is equal to that of the observation. The fact that only the dispersion is quantified is one of the major drawbacks of r^2 if it is considered alone. A model which systematically over or underpredicts all the time will still result in good r^2 values close to 1.0 even if all predictions were wrong. By weighting r^2 by the slope of regression line between observed and predicted, under or overpredictions are quantified together with the dynamics which results in a more comprehensive reflection of model results. We used a slightly modified weighted r^2 as originally introduced by *Krause et al*. [2005] as the efficiency criterion for discharge and nitrate

$$\phi = \begin{cases} br^2 & \text{for} \quad b \le 1 \\ b^{-1}r^2 & \text{for} \quad b > 1 \end{cases} \tag{2}$$

where r^2 is the coefficient of determination and b is the slope of the regression line between the simulated and measured data. For a good agreement the interception of the regression line should be close to zero which means that an observed runoff of zero would also result in a prediction near zero and the gradient b should be close to one. For multiple outlets and attributes, the objective function Φ was expressed as

$$\Theta = \frac{1}{w_{v1}+w_{v2}} \left[\frac{w_{v1}}{\sum_{i=1}^{n_1} w_i} \sum_{i=1}^{n_1} w_i \phi_i + \frac{w_{v2}}{\sum_{i=1}^{n_2} w_i} \sum_{i=1}^{n_2} w_i \phi_i \right] \tag{3}$$

where w_{v1} and w_{v2} are weights of the two variables, n_1 and n_2 are the number of discharge and nitrate stations, respectively, and w_i's are the weights of variables at each station. The function ϕ and consequently Θ vary between 0 and 1. The best simulation is considered the one with the highest Θ value. A major advantage of br^2 efficiency criterion is that it ranges from 0 to 1, which compared to Nasch-Sutcliff Efficiency coefficient, ensures that in a multisite multiattribute calibration, the objective function is not dominated by a few bad results. Weights in equation (3) would be critical if an objective function such as mean square error was used, but because of using br^2 they did not make any significant difference to model calibration results. For this reason, we set them to 1. For crop yield we used mean square error as the objective function after an initial calibration of model for discharge and nitrate

$$\phi_3 = \frac{1}{n_3} \sum_{i=1}^{n3} \left(Y_i^o - Y_i^s \right)^2 \tag{4}$$

where n_3 is the number of sites with wheat, barley, and corn yield data, Y^o (t ha^{-1}) is the observed yield, and Y^s (t ha^{-1}) is the simulated yield.

A few iterations are then carried out seeking to reach an optimal *P-factor* and *R-factor* until a further improvement in the objective function is not found. As mentioned before, the calibration runs were made using parallel SUFI-2 [*Rouholahnejad et al.*, 2012] and the grid-based SWAT (gSWAT) [*Gorgan et al.*, 2012]. As SUFI-2 is a sequential procedure, several iterations of 200 simulations each were performed for calibration.

3. Results and Discussion

The model response to various land uses and climate data was tested by comparing simulated river discharges against the observation. For land use, our analysis indicated that classification and resolution did not have a significant effect on river discharge simulation in the BSB model. MODIS land cover was used in the final SWAT project as it produced relatively better discharge results. As model calibration started far back in time, we also tested the model by changing the land use during SWAT simulation. We found that the impact of historic land use change on our large-scale model results was negligible and, hence, did not consider this change during calibration.

We also found that CRU-based simulated discharges performed significantly better in the project as compared to simulated discharges based on measured climate stations. This could be because the climate stations suffered from a large amount of missing data, different data qualities, and uneven distribution throughout the region. Subsequently, the CRU data set was selected to model the hydrology of the BSB.

SWAT calculates the rainfall and temperature of each subbasin using the nearest climate station to the centroid of that subbasin. As rainfall is the most important driving variable in a hydrological model, when comparing the results of this work with other works, it is important to have the distribution of the rainfall in mind (Figure 2). Differences are observed in the coefficients of variation (CV) of long-term annual precipitation and temperature averages (1973–2006) across the BSB. This indicates the degree of year to year

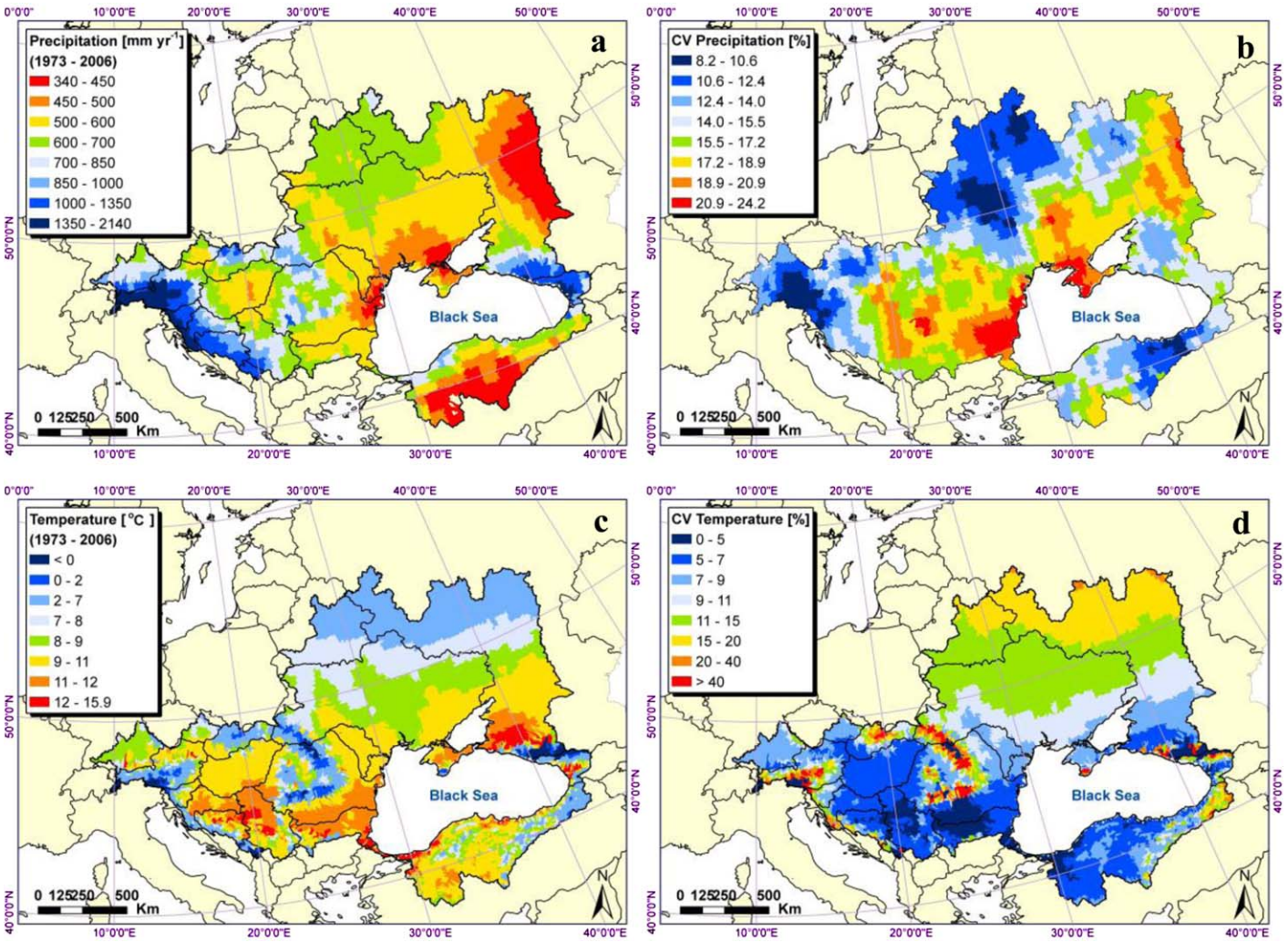

Figure 2. Long-term annual average (1973–2006) precipitation and average temperature distribution across Black Sea Basin based on the CRU data set. Also shown are the coefficients of variation indicating the temporal variability of precipitation and average temperature.

variability during the simulation period. This variation has an influence on the prediction uncertainties of all water cycle components as we will see later for the case of Bulgaria and Turkey.

3.1. Calibration and Uncertainty Analysis

3.1.1. Examining Model Setup

Initially, a broad set of parameters were used for discharge calibration [*Holvoet et al*., 2005; *Wang et al*., 2005, *Abbaspour et al*., 2007; *Faramarzi et al*., 2009]. Then a sensitivity analysis was performed to identify the key parameters across BSB, which led to selection of 20 parameters integrally related to stream flow (Table 1). Although the initial parameter ranges were as wide as physically meaningful, some outlets were still completely outside of the 95PPU range. These outlets would obviously not benefit from parameter calibration alone. We investigated the poorly simulated outlets one by one using the visualization module of SWAT-CUP. This involves projection of the study area on the Microsoft's BING map to identify the reasons for the inadequate simulations. In the visualization module, we observe the subbasins, outlet positions, simulated rivers, and climate stations from the SWAT project, as well as landcover and other layers of information in the BING map. Several problems were discovered, which are inevitable in a large-scale projects and needed careful attention.

Examples of these include positioning the outlets on a wrong rive (Figures 3a and 3b). As SWAT connects each measured outlet to the nearest rivers, any errors in the coordinates of outlets can cause a wrong

Table 1. List of Parameters and Their Initial Ranges Used for Model Calibration

Parameter Name	Definition	Initial Range
r__CN2.mgt	SCS runoff curve number for moisture condition II	−0.35 to 0.35
r__ALPHA_BF.gw	Base flow alpha factor (days)	−0.8 to 0.8
r__GW_DELAY.gw	Groundwater delay time (days)	−0.8 to 0.8
r__GWQMN.gw	Threshold depth of water in shallow aquifer for return flow (mm)	−0.8 to 0.8
r__GW_REVAP.gw	Groundwater revap. coefficient	−0.4 to 0.4
r__REVAPMN.gw	Threshold depth of water in the shallow aquifer for "revap" (mm)	−0.4 to 0.4
r__RCHRG_DP.gw	Deep aquifer percolation fraction	0.3 to 0.5
r__CH_N2.rte	Manning's *n* value for main channel	−0.8 to 0.8
r__CH_K2.rte	Effective hydraulic conductivity in the main channel (mm h^{-1})	−0.8 to 0.8
r__ALPHA_BNK.rte	Base flow alpha factor for bank storage (days)	−0.6 to 0.6
r__SOL_AWC().sol	Soil available water storage capacity (mm H_2O/mm soil)	−0.5 to 0.5
r__SOL_K().sol	Soil conductivity (mm h^{-1})	−0.8 to 0.8
r__SOL_BD().sol	Soil bulk density (g cm^{-3})	−0.4 to 0.4
r__SFTMP().sno	Snowfall temperature (°C)	−0.4 to 0.4
r__SMTMP().sno	Snow melt base temperature (°C)	−0.4 to 0.4
r__SMFMX().sno	Maximum melt rate for snow during the year (mm $°C^{-1}$ d^{-1})	−0.4 to 0.4
r__SMFMN().sno	Minimum melt rate for snow during the year (mm $°C^{-1}$ d^{-1})	−0.4 to 0.4
r__SLSUBBSN.hru	Average slope length (m)	−0.4 to 0.4
r__OV_N.hru	Manning's *n* value for overland flow	−0.4 to 0.4
r__HRU_SLP.hru	Average slope steepness (m m^{-1})	−0.4 to 0.4
r__CMN.bsn	Rate factor for humus mineralization of active organic nitrogen	−0.4 to 0.4
r__NPERCO.bsn	Nitrogen percolation coefficient	−0.4 to 0.4
r__N_UPDIS.bsn	Nitrogen uptake distribution parameter	−0.4 to 0.4
r__RCN.bsn	Concentration of nitrogen in rainfall (mg N L^{-1})	−0.4 to 0.4
r__SHALLST_N.gw	Concentration of nitrate in groundwater to streamflow (mg N L^{-1})	−0.4 to 0.4

placement. This perhaps leads to the biggest calibration problem. As shown in Figure 3b, the outlet is placed on a tributary of the Danube called Tamis near Pancevo in Serbia. The black dashed line near the *x* axis (Figure 3c) is simulated river discharge before correcting the location, and the red line shows simulated discharge after correcting the location.

Other major problems result from an outlet being positioned downstream of a reservoir. In particular, in Southern Bug in Ukraine, the simulated discharge and observations match quite well until the Alexandra

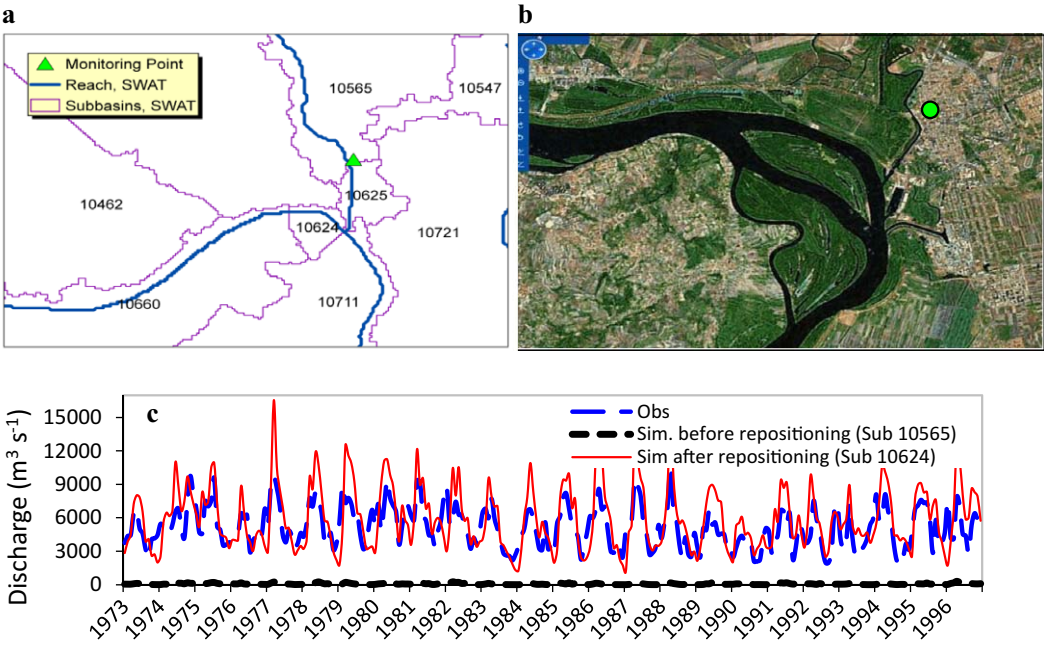

Figure 3. Example of a wrong positioning of the outlets due to errors in the reported coordinates of the measurement stations. The outlet's correct position is on the Danube River (upstream area of 497,500 km^2) rather the Tamis River (upstream area of 16,460 km^2), a tributary of the Danube.

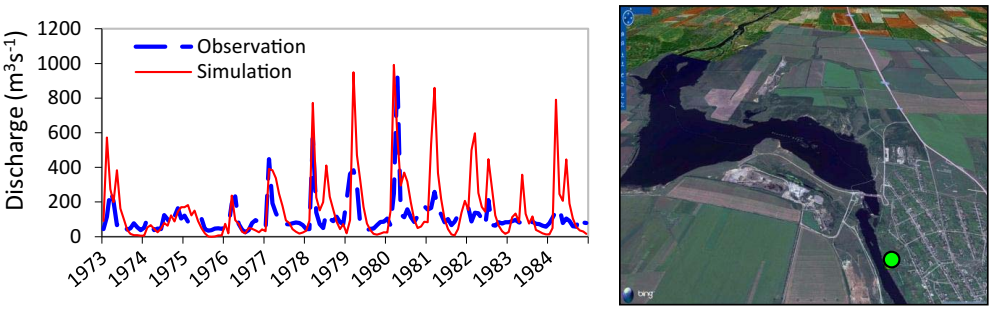

Figure 4. Example of an outlet being at the downstream of a reservoir. In the Southern Bug in Ukraine (upstream area of 45,180 km^2), Alexandra Reservoir came into operation in 1979. There is a clear change in the discharge pattern after the operation of the reservoir which could not be captured by the model.

Reservoir came into operation in 1979 (Figure 4). Clearly the dynamics of such outlets depend on the management of the reservoir and not natural processes. Other problematic situations may arise when outlets are in a highly populated or agricultural region where water management and water transfers are large. In these situations also, SWAT cannot be expected to produce proper results unless data are available. Constructions of dams for irrigation and power generation purposes as well as other water management practices such as water abstraction and diversion create major difficulties for model calibration. As management information are usually not available, proper cautions need to be taken during calibration. These include converting outlets to inlets, weighing those outlets under the influence of management less in the objective function, or removing the outlets downstream of reservoirs from the calibration process. Because of lack of water management data, we excluded from calibration those outlets directly affected by infrastructures such as dams and reservoirs. After making appropriate corrections to badly simulated outlets and obtaining relatively satisfactory discharge estimation, nitrate parameters (Table 1) were added to the parameter pool.

3.1.2. Parameterization

In subsequent iterations the model was parameterized. Parameterization refers to regionalization of parameters tailored to achieve the best response from the simulation program and individual outlets. Some examples are if there is an early shift in the simulation (Figure 5a), then decreasing the overland flow (HRU_SLP) by 10–20%, increasing Manning's roughness coefficient (OV_N) by 10–30%, and increasing the flow length (SLSUBBSN) by 5–15 m in all the upstream subbasins of that outlet will improve the simulated discharge. Accordingly, if the simulated base flow is too high (Figure 5b), then parameterization includes: increasing deep percolation loss (GWQMN), increasing groundwater revap coefficient (GW_REVAP) to a maximum of 0.4, and decreasing the threshold depth of water in shallow aquifer (REVAPMN) to a minimum of zero. In another example, if the simulated peak flow is underestimated (Figure 5c), then the following adjustments to the upstream subbasins of that outlet should be made: increasing the curve number (CN2) by 10–15%, decreasing the soil available water storage capacity (SOL_AWC) by 5–10%, and decreasing the soil evaporation compensation factor (ESCO) by 20–30%. This will ensure a better simulation at the specified outlet. For every outlet, the upstream subbasins were parameterized as described above.

3.1.3. Calibration Performance

The final calibration results for outlets that were used in model calibration range from very good to poor (Figure 1). The bR^2 statistic for discharge outlets range from 0.2 to 0.8 and for nitrate outlets from less than 0.1 to 0.7. The time series examples (Figure 6) for two outlets show good results in both calibration and validation periods.

It is important to note that the 95PPU represents model prediction and not the "best simulation." The latter is only provided for reference. Calibration is concerned with the problem of making inferences about physical systems from measured output variables of the model (e.g., river discharge, nitrate load, etc.). Because nearly all measurements are subject to some uncertainty, the inferences are usually statistical in nature. Furthermore, because one can only measure a limited number of (noisy) data and because physical systems are usually modeled by continuum equations, no calibration problem is really uniquely solvable [*Abbaspour et al*., 2007]. In calibration, therefore, we characterize the set of models, mainly through assigning distributions (uncertainties) to the parameters that fit the data. We should also make the distinction here between

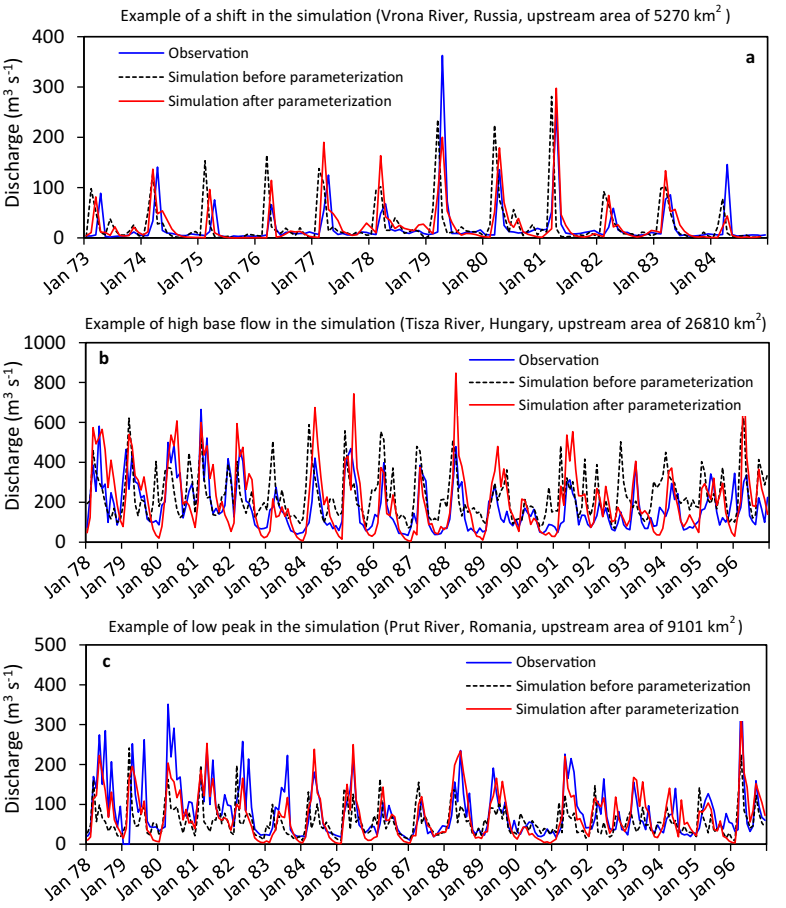

Figure 5. Examples of parameterization. Simulations are discrepant in terms of a shift, higher base flow, or lower peaks. In each case, relevant parameters are changed in all the upstream subbasins.

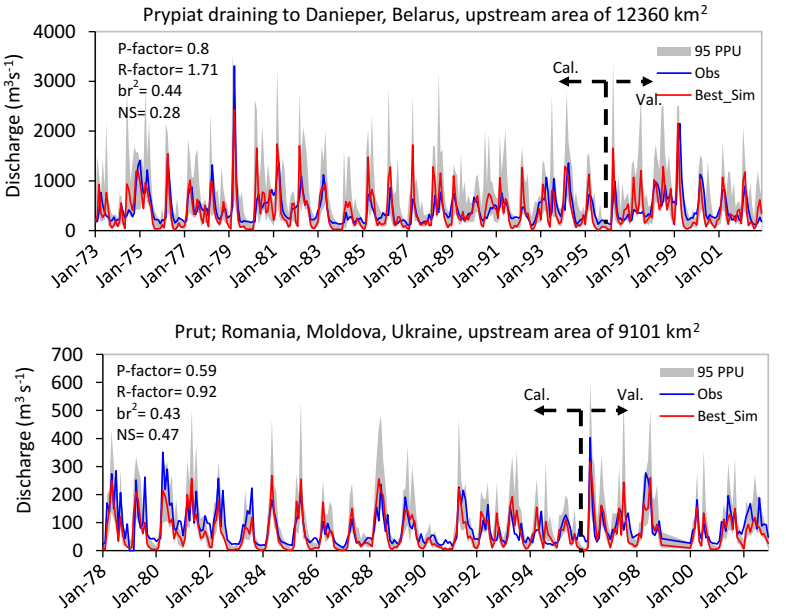

Figure 6. Comparison of simulated and observed discharges at Prypiat and Prut rivers for calibration and validation periods. The shaded region is 95% prediction uncertainty band. The best model simulation is also shown by the red line. The reported statistics are for the entire simulation period.

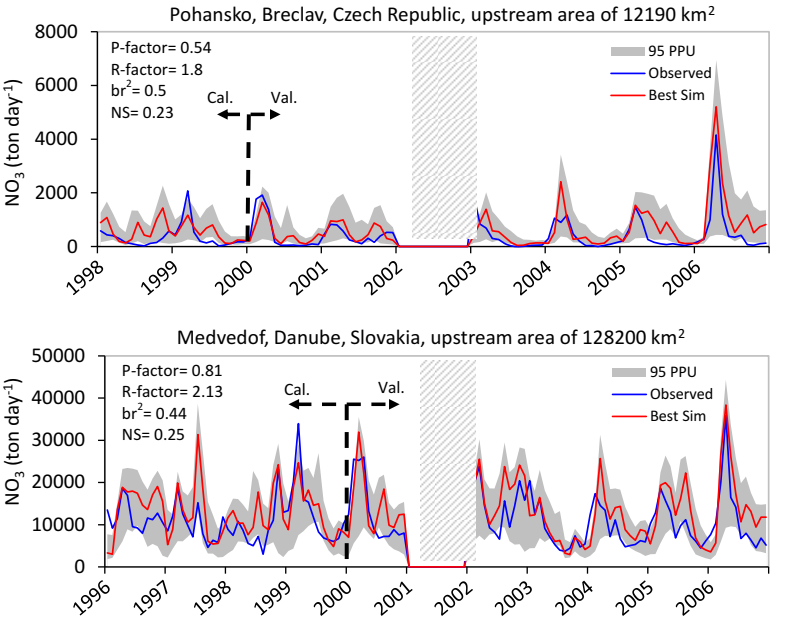

Figure 7. Comparison of simulated and observed nitrate loads in Dyje River in Czech Republic and Danube River in Slovakia for calibration and validation periods. The shaded region is 95% prediction uncertainty band. The best model simulation is also shown by the red line. The reported statistics are for the entire simulation period.

uncertainty and error. Prediction uncertainty arises from the uncertainty in the parameters, in the model, and in the inputs. In the concept of SUFI-2, all these uncertainties are assigned to the parameter distributions. The uncertainty is expressed as the 95PPU, which as stated above is also the output of the model (Figure 6). Model error, however, is the degree in which the 95PPU does not account or does not bracket the observation. This, in SUFI-2, is indicated by (1-*P-fcator*), which is around 20% for Daniper and 41% for Prut River (Figure 6). A closer examination of the Prut River simulation reveals that most of the error originates from the base flow simulation. Hence, the processes related to surface water-ground water interaction are not very well represented in the model in that region.

For a model to better represent a region of study we could introduce more attributes in the objective function. In this research, we used nitrate load as well as crop yield to achieve a model with more confidence in predicting the water balance components.

Water quality was simulated through nitrate loads in rivers. We were disappointed at the lack of more easily available information in the BSB, especially with respect to water quality. Most of the information we gathered came from the Danube River Basin; therefore, the water quality component of the Black Sea model should be considered as uncalibrated or at best partially calibrated for other river basins within the BSB. The simulations, however, were surprisingly satisfactory for most stations given that we had estimated the point sources and had only rough data with respect to diffuse sources of pollution in different countries (Figure 7). It is expected that nitrate simulation would be accompanied by much large prediction uncertainty due to larger uncertainty in the input data for point and diffuse sources. An interesting observation is the overestimation of the model at the stations near Danube Delta. As the river approaches the Delta, the concentration of nitrate decreases, but the model cannot account for this because deltas and wetlands are not represented in SWAT (Figure 8).

Because of a direct relationship between crop yield and evapotranspiration [*Jensen*, 1968; *FAO*, 1986], in addition to nitrate loads, we included yields of maize, barley, and wheat as extra target variables in the calibration process. With measured river discharges we can obtain a good knowledge of runoff, but cannot have any confidence with respect to soil moisture, evapotranspiration, or aquifer recharge. Knowledge of evapotranspiration through simulation of crop yield could, therefore, increase our confidence in soil moisture and aquifer recharge. Average annual yield of three major crops (barley, maize, and wheat) are simulated at subbasin level and aggregated per country for the duration of 1973–2006 and expressed as 95%

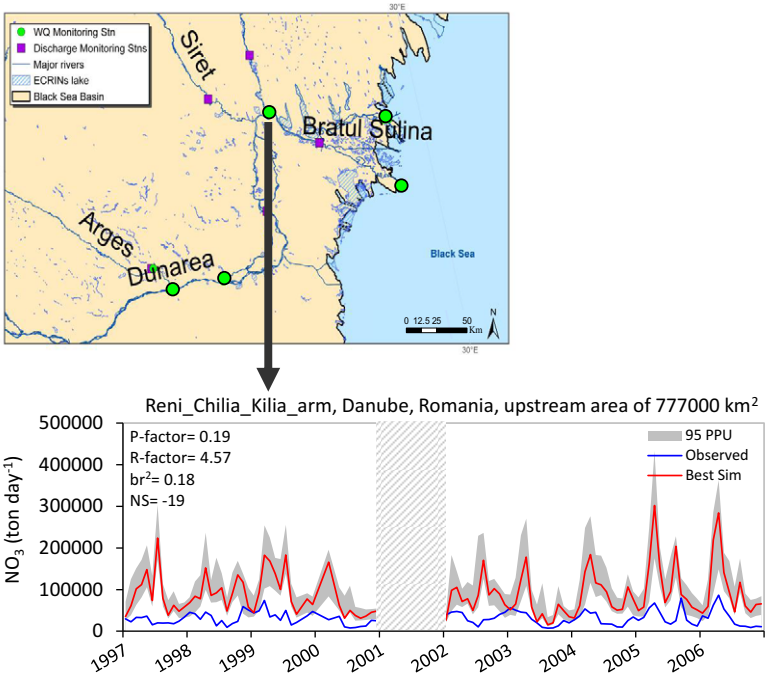

Figure 8. Decrease in river load as it enters the Danube Delta. Observation shows much lower load than model simulation since deltas and wetland processes are not accounted in the model.

prediction uncertainty (Figure 9). The FAO yield data and the data from the McGill University fall inside or are close to the predicted bands. We note that the actual uncertainty should perhaps be larger than what we have reported here. In the final iteration some crop parameters (e.g., heat unit, harvest index, biomass target, etc.) were fixed to values obtained by manual calibration for the entire country and were not treated as uncertain. Crop parameters were parameterized based on crop type, management operation (e.g., planting time, harvest time, irrigation, fertilization, etc.), and region-specific operations, resulting in a large number of parameters. Their inclusion in the uncertainty analysis would require a large number of simulations, which was not feasible in the time span of the project. The discrepancies between the simulated and the reported yields could be due to a lack of knowledge of detailed agricultural management in different regions in our model, but also errors in the observed data, as there were also differences in the reported yields of FAO and McGill databases (Figure 9).

3.2. Quantification of Water Resources and Their Respective Uncertainties

We used the calibrated BSB model to calculate water resources components: blue water, green water flow, and green water storage. These concepts give an overall picture of water resources and bring the outputs of the BSB model closer to the needs of water resources researchers and policy makers. The upper and lower bounds of the 95% prediction uncertainties for the blue water (Figures 10a and 10b) show a wide range in some regions indicating the importance of uncertainty analysis in hydrological modeling. This uncertainty reflects primarily the prediction uncertainty (including model, parameters, and inputs) as well as the temporal climate variation as a secondary effect. The temporal variation is depicted by the coefficient of variation (CV) in Figure 10d. The simulated daily water fluxes have been accumulated on the annual basis and averaged for the years 1973–2006 at the subbasin level (Figure 10c). The latter map shows the distribution of the average annual freshwater availability. It is basically the water yield to stream flow from HRUs in the watershed (e.g., surface runoff, plus the lateral flow to the river, plus the shallow aquifer contribution to the rivers, minus pond abstraction and transmission losses) plus deep aquifer recharge. Transmission losses reflect the water lost from tributary channels in the HRUs via transmission through the bed.

Green water components are illustrated in Figure 11 along with their CVs. In each case, there are large spatial variations across the Basin. CV depicts the temporal variation and it is seen that green water storage or

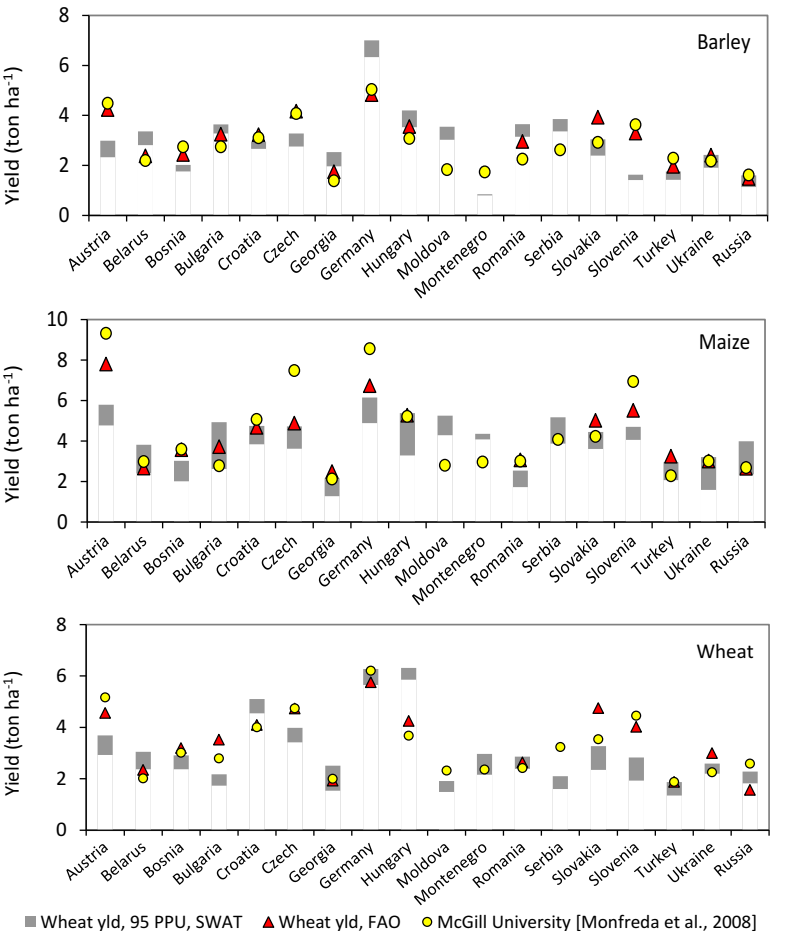

Figure 9. Subbasin yields are aggregated per country to compare with FAO's statistical reports and the report by McGill University. Some model discrepancies are due to lack of knowledge of detail management operations in different countries.

soil moisture is relatively less variable temporally in many regions. This indicates a higher reliability of this resource over time, and hence, a less risky opportunity for development of green, or rain-fed agriculture.

The confidence on water resources estimates is relatively high because surface runoff as well as evapotranspiration (through crop yield) was satisfactorily calibrated in the model. For a further comparison with the reported literature we calculated the freshwater availability on country basis and compared them to the values of FAO (Figure 12). The simulation results are expressed as 95% prediction uncertainty bands. It is seen that the FAO-estimated water availability fall inside or are very close to the simulation 95PPU band in all countries. Summary of water resources for major BS countries are presented in Table 2. Georgia is shown to have the largest blue water in mm yr^{-1}, and Bulgaria the smallest.

Knowledge of the long-term time series of water availability is very important in water management and planning studies, water transfers, reservoir operation, and conjunctive water analyses. Many countries have large monthly variabilities in the blue and green water components as illustrated, for example, by the long-term monthly variations in Turkey and Bulgaria (Figure 13). It is interesting to note that soil moisture (green water storage) is larger in Bulgaria than in Turkey, while Turkey's blue water is larger. We could conclude that as a whole, runoff is larger in Turkey, while the share of infiltration is greater in Bulgaria. The large uncertainty in green water storage in Bulgaria appears to be dominated by large annual variation in precipitation (Figure 2b).

3.3. Transboundary Rivers

As measurements cannot be made at all transboundary points and for all variables, models can play an important role. We use the example of Dniester River to show the ability of the model to address some

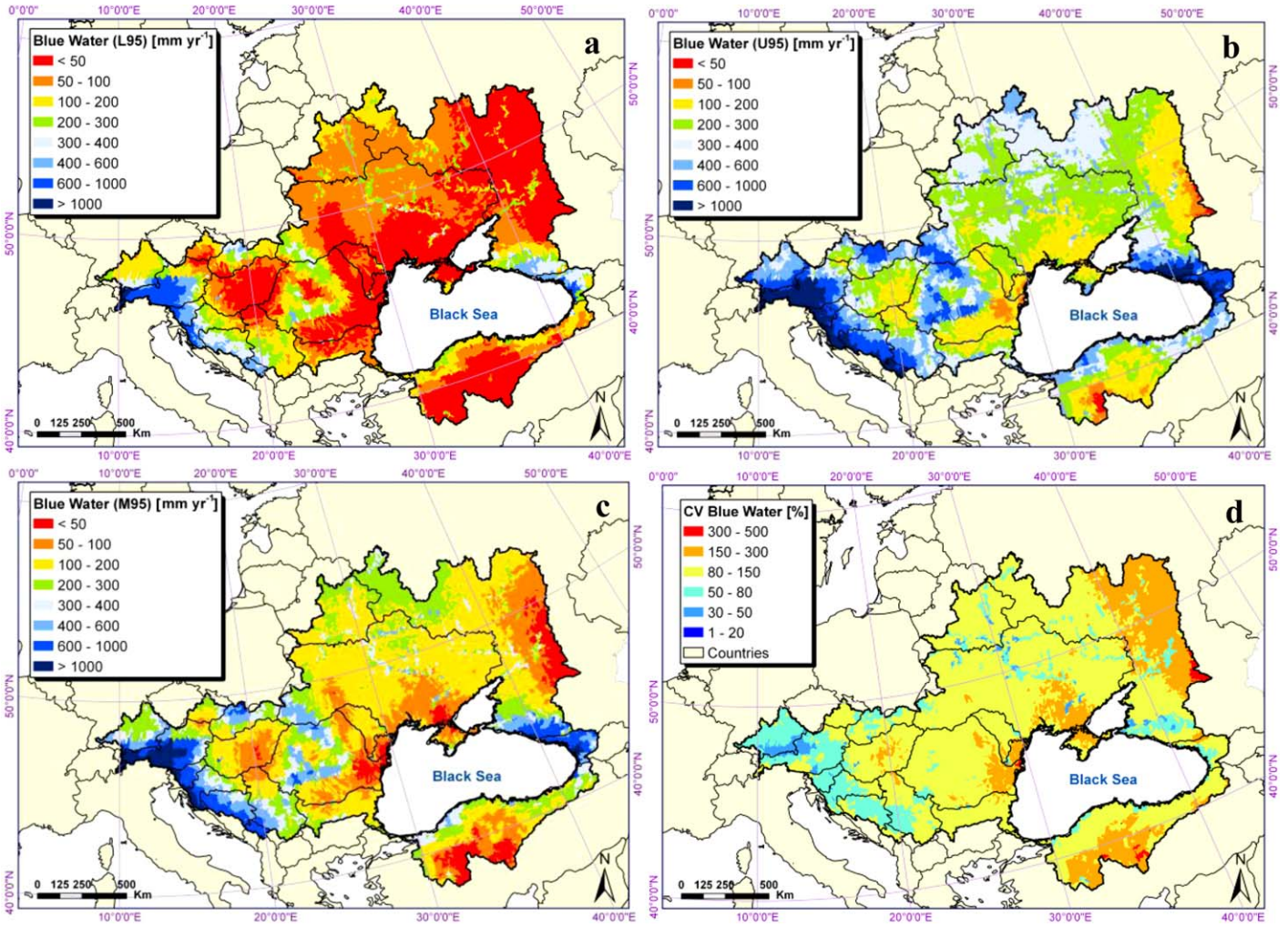

Figure 10. Annual averages of blue water at 12,982 modeled subbasins of Black Sea Basin expressed as (a) lower (L95), (b) upper (U95), and (c) median (M95) of the 95% prediction uncertainty range, (d) coefficient of variation indicating temporal flocculation calculated for the period of 1973–2006.

transboundary issues. Dniester (1380 km) has its source in the Carpathian Mountains in Ukraine, flowing south and east along the territory of Moldova, and re-entering Ukraine near the Black Sea coast (Figure 14a). Dniester is the main source of drinking water in Moldova and is no less important for a significant part of Ukraine, particularly the Odessa Region. Hydropower is one of the major sectors affecting the ecological status of the Dniester Basin. The Dniester flow in its middle section was dammed to fill a chain of reservoirs, the largest of them being the Dubossary (1954) and Dniestrovsky (1983) reservoirs. Large areas of intensive irrigated agriculture, both in Ukraine and Moldova, and soil erosion contribute significantly to the contamination of water bodies by nutrients and chemical fertilizers [*OSCE/UNECE*, 2005].

The simulation of discharge and nitrate loads just before the Dniester River enters Moldova and right after it leaves the country (Figures 14b and 14c) shows an increase in the discharge with larger peaks as well as a significant increase in nitrate load as the river leaves Moldova. Such analyses can serve as important instruments in resolving transboundary conflicts and lead to a better management of the transboundary rivers.

4. Summary and Conclusion

In this study, we aimed for building a high-resolution hydrological model for the Black Sea Basin. The objective was to quantify water resources availability and water quality in terms of nitrate load at subbasin spatial

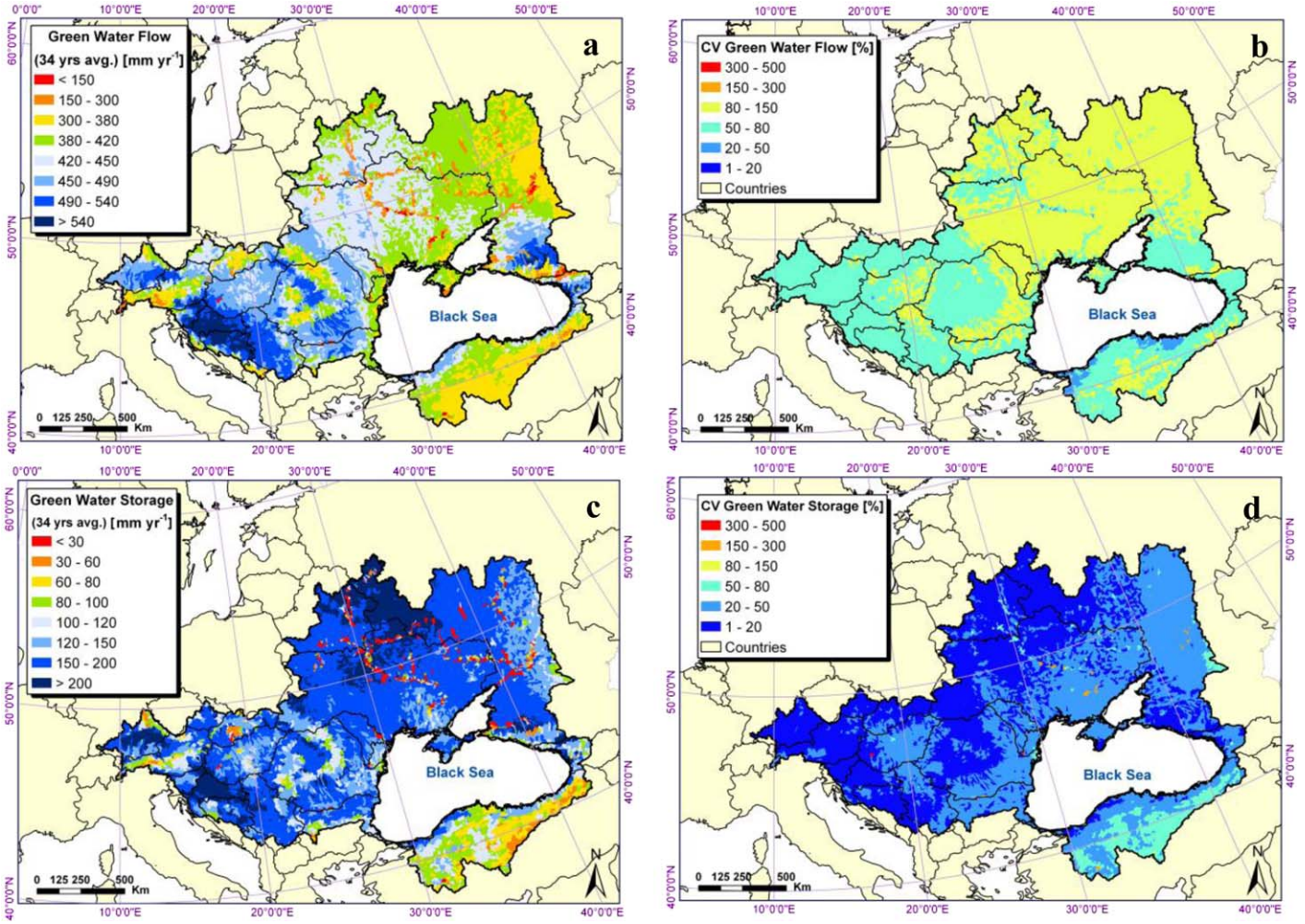

Figure 11. (a, c) Long-term annual averages (1973–2006) of green water flow and green water storage at subbasin level in the Black Sea Basin. (b, d) The coefficients of variation (CV) on the right show the temporal variability in each component (1973–2006). A low CV indicates a higher reliability of that resource.

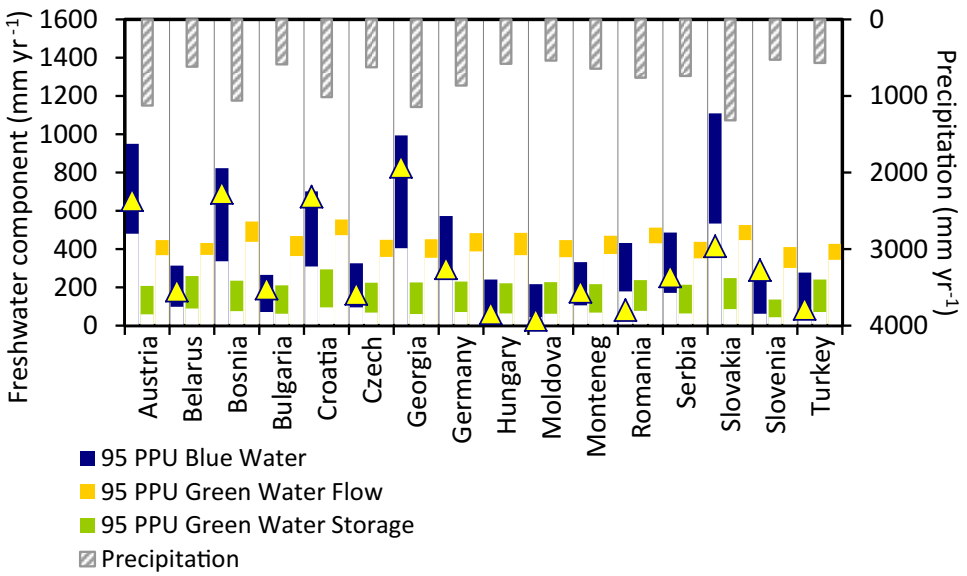

Figure 12. Comparison of simulated average annual freshwater availability (blue water, green water flow, and green water storage) per country for the duration of 1973–2006 expressed as 95% prediction uncertainties and precipitation. FAO estimates on internal renewable water resources (blue water) are provided as a comparison.

Table 2. Fresh Water Availability and Per Capita Water Resources of Black Sea Basin Countries[a]

Country	Area (km^2)	Precipitation (mm yr^{-1})	Blue Water (mm yr^{-1})	Green Water Flow (mm yr^{-1})	Green Water Storage (mm)	Per Capita Blue Water Availability (m^3 capita^{-1} yr^{-1})
Austria	83,870	1124	481–951	369–448	60–208	5,331–10,544
Belarus	202,900	617	99–315	371–432	89–260	3,292–10,455
Bosnia	51,129	1059	338–823	438–545	77–236	5,686–13,865
Bulgaria	108,489	585	72–265	364–469	63–212	1,667–6,167
Croatia	55,974	1015	309–702	473–555	96–295	5,967–13,549
Czech	79,000	627	96–327	360–448	68–224	2,833–9,589
Georgia	70,000	1144	406–995	355–452	61–226	13,683–33,572
Germany	357,022	862	242–574	389–483	72–231	9,012–21,388
Hungary	93,030	579	46–242	368–486	64–223	443–2,337
Moldova	33,843	536	44–218	358–448	63–228	358–1,769
Romania	238,300	643	106–333	375–470	68–217	1,168–3,648
Serbia	102,350	760	180–433	431–513	78–238	2,114–5,093
Slovakia	48,845	739	172–487	352–438	65–214	1,638–4,643
Slovenia	20,253	1319	534–1,109	448–527	86–249	5,427–1,1267
Turkey	780,000	526	63–269	302–412	44–137	1,850–7,883
Ukraine	603,000	568	73–279	344–427	72–242	959–3,676
Russia	1,719,712	564	74–306	326–407	71–241	5,654–23,271

[a]Precipitation is presented as the average rainfall in the simulation period. The 95% prediction uncertainty ranges are shown for water resources components. The lower and upper bounds are averaged over the period of 1973–2006.

and monthly temporal level. We used the SWAT model for this purpose and calibrated the model using SUFI-2 algorithm, which ran on a grid network. The calibration was based on river discharge, crop growth, and river nitrate load at multiple sites. As there are often no data on soil moisture, evapotranspiration, or

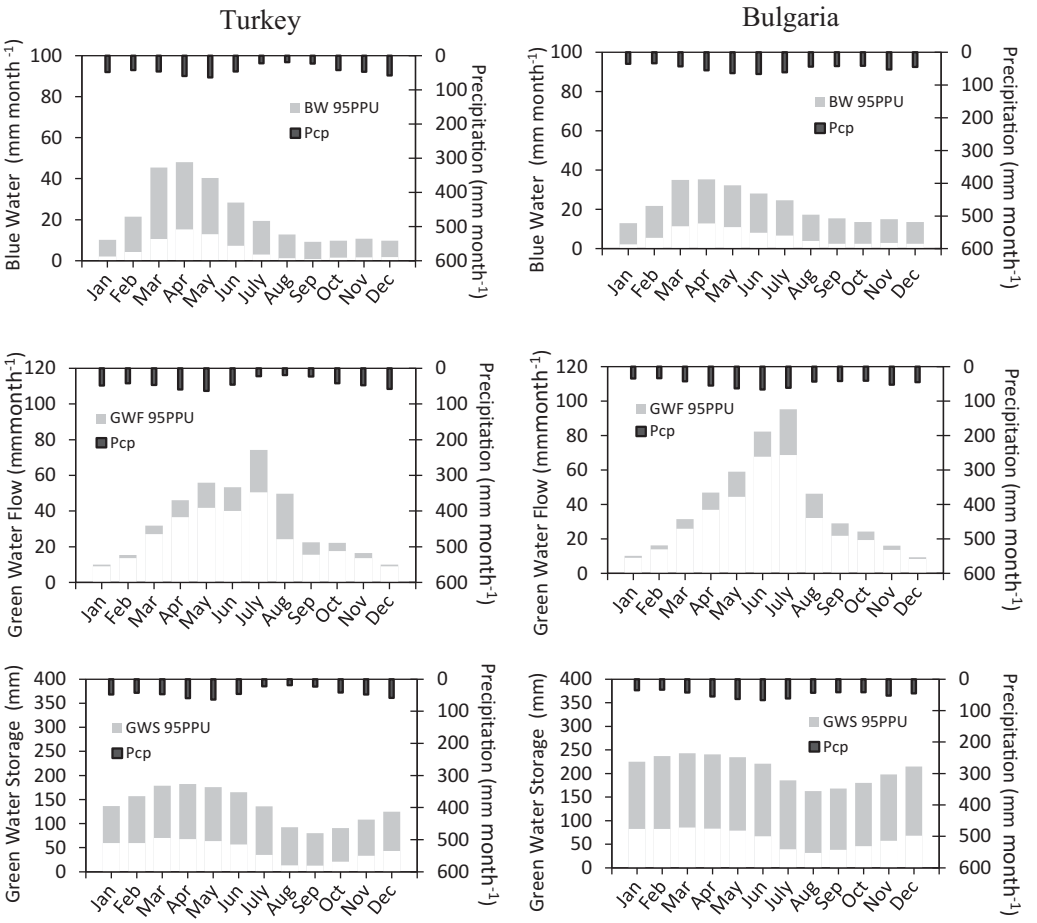

Figure 13. Average (1973–2006) monthly 95% prediction uncertainty distributions of fresh water availability components (blue water, green water flow, and green water storage) in Turkey and Bulgaria.

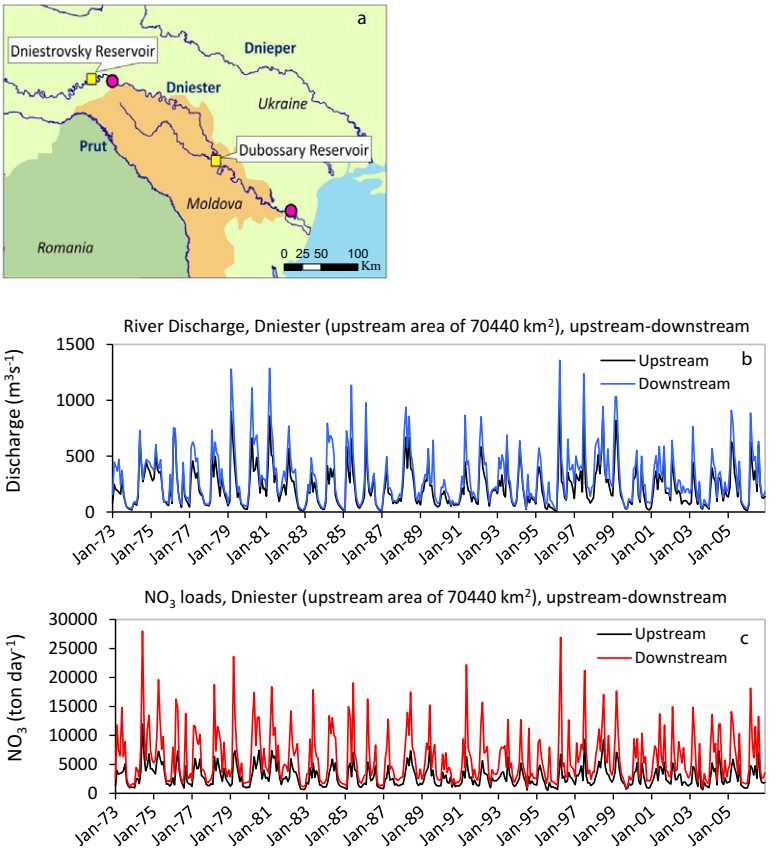

Figure 14. Dnieper Transboundary River crossing Ukraine-Moldova boarder and entering Ukraine again. Discharges and nitrate loads are shown at the entry (upstream) and exit (downstream) points in Moldova.

aquifer recharge, we used crop yield as a surrogate to add confidence on the distribution of the components of the infiltrated water. The calibration and validation results were quite satisfactory for a large number of outlets for both discharge and nitrate loads. As a consequence, our confidence on the estimated water resources is high. However, as nitrate data were only available for the Danube Basin, nitrate load estimation at other areas should be considered as less reliable.

The model output included blue water flow, green water flow, and green water storage as well as nitrate load, and crop yields. We identified water scarce regions and showed how the model could provide information on transboundary water issues such as natural flows and pollution loads. Regions in Ukraine and Romania bordering the Black Sea and parts of Turkey and Russia in the Basin experience the highest water deficit. Model outputs could be used to establish environmental goals, planning of remedial measures and development of monitoring strategies. Much more results and analysis could be obtained with the model developed in this study, such as calculation of freshwater and nutrient fluxes in to the Sea. In the next phase of the study, we will use results of land use and climate change models to describe variability in hydrological water balance and nutrient load for future conditions.

Based on the results of this study, we conclude that given the present technologies it is possible to build a high resolution model of a large basin. What could provide more confidence in the model result are more discharge and water quality data (nitrate, phosphate, sediment, etc.) and higher-resolution crop yield data for model calibration.

Acknowledgments
This project has been funded by the European Commission's Seventh Research Framework through the enviroGRIDS project (grant agreement 226740). The authors are especially grateful to Envirogrid partners for contributing data to this project: Alex Hebort from International Commission for the Protection of the Danube River (ICPDR), Gencay Serter from Turkish Ministry of Forest and Water Affairs (MEF), Romanian National Institute of Hydrology and Water Management (INHGA), Danube Delta National Institute for Research and Development (DDNI) in Romania. Special thanks to Dorian Gorgan and his team in Cluje Technical University for their support on calibration execution on grids. We are also grateful to Rainer Schulin from ETH Zurich University for their valuable comments and discussions for this work.

References

Abbaspour, K. C. (2011), *User Manual for SWAT-CUP, SWAT Calibration and Uncertainty Analysis Programs*, 103 pp., Eawag: Swiss Fed. Inst. of Aquat. Sci. and Technol., Duebendorf, Switzerland. [Available at http://www.eawag.ch/forschung/siam/software/swat/index.]

Abbaspour, K. C., C. A. Johnson, and M. Th. van Genuchten (2004), Estimating uncertain flow and transport parameters using a sequential uncertainty fitting procedure, *J. Vadose Zone*, *3*(4), 1340–1352.
Abbaspour, K. C., J. Yang, I. Maximov, R. Siber, K. Bogner, J. Mieleitner, J. Zobrist, and R. Srinivasan (2007), Modelling hydrology and water quality in the pre-Alpine/Alpine Thur watershed using SWAT, *J. Hydrol.*, *333*, 413–430, doi:10.1016/j.jhydrol.2006.09.014.
Alcamo, J., P. Döll, T. Henrichs, F. Kaspar, B. Lehner, T. Rösch, and S. Siebert (2003), Development and testing of the WaterGAP 2 global model of water use and availability, *Hydrol. Sci. J.*, *48*(3), 317–338.
Arnold, J. G., R. Srinivasan, R. S. Muttiah, and J. R. Williams (1998), Large area hydrologic modeling and assessment part I: Model development, *J. Am. Water Resour. Assoc.*, *34*(1), 73–89.
Aus der Beek, T., L. Menzel, R. Rietbroek, L. Fenoglio-Marc, S. Grayekd, M. Becker, J. Kusche, and E. V. Stanev (2012), Modeling the water resources of the Black and Mediterranean Sea river basins and their impact on regional mass changes, *J. Geodyn.*, *59–60*, 157–167.
Black Sea Investment Facility (BSEI) (2005), Review of the Black Sea Environmental Protection Activities, general review.
Center for International Earth Science Information Network (CIESIN) (2005), Gridded Population of the World: Future Estimates (GPWFE), Socioecon. Data and Appl. Cent., Columbia Univ., N.Y. [Available at http://sedac.ciesin.columbia.edu/gpw.]
Climatic Research Unit (CRU) (2008), CRU Time Series (TS) High Resolution Gridded Datasets, NCAS Br. Atmos. Data Cent., U. K. [Available at http://badc.nerc.ac.uk/view/badc.nerc.ac.uk__ATOM__dataent_1256223773328276.]
Döll, P., F. Kaspar, and B. Lehner (2003), A global hydrological model for deriving water availability indicators: Model tuning and validation, *J. Hydrol.*, *270*(1–2), 105–134.
Dumont, E., R. Williams, V. Keller, A. Voss, and S. Tattari (2012), Modelling indicators of water security, water pollution and aquatic biodiversity in Europe, *Hydrol. Sci. J.*, *57*, 1378–1403.
European Environmental Agency (EEA) (2010), The European environment—State and outlook 2010: Synthesis, *State Environ. Rep. 1/2010*, 533, Copenhagen.
EEA Catchments and Rivers Network System (ECRINS) v1.1 (2012), Rationales, building and improving for widening uses to Water Accounts and WISE applications, *Tech. Rep. 7/2012*, Eur. Environ. Agency, Copenhagen.
Environmental Space Agency (ESA) (2008), The GlobCover Project, led by MEDIAS-France, France. [Available at http://due.esrin.esa.int/globcover.]
Environmental Space Agency (ESA) (2010), The GlobCorine Project, led by Université Catholique de Louvain, Belgium. [Available at http://dup.esrin.esa.int/ionia/globcorine/products.asp.]
Falkenmark, M., and J. Rockström (2006), The new blue and green water paradigm: Breaking new ground for water resources planning and management, *J. Water Resour. Plann. Manage.*, *132*(3), 129–132.
Faramarzi, M., K. C. Abbaspour, R. Schulin, and H. Yang (2009), Modelling blue and green water resources availability in Iran, *J. Hydrol. Processes*, *23*, 486–501, doi:10.1002/hyp.7160.
Food and Agricultural Organization (FAO) (1986), Early agrometeorological crop yield forecasting, *FAO Plant Prod. Prot. Pap. 73*, edited by M. Frère and G. F. Popov, Rome.
Food and Agricultural Organization (FAO) (1995), *The Digital Soil Map of the World and Derived Soil Properties* [CD-ROM], Version 3.5, Rome.
Food and Agricultural Organization Statistics (FAOSTAT) (2013), Statistic devision of Food and Agricultural Organization, Rome, Italy. [Available at http://faostat3.fao.org/faostat-gateway/go/to/home/E.]
Gassman, P. W., M. R. Reyes, C. H. Green, and J. G. Arnold (2007), The soil and water assessment tool: Historical development, applications, and future research directions, *Trans. ASABE*, *50*, 1211–1250.
Global International Waters Assessment (GIWA) (2005), *Transboundary Waters in the Black Sea-Danube Region*, 53 pp., Univ. of Kalmar, Kalmar, Sweden.
Global Runoff Data Centre (GRDC) (2011), Long-Term Mean Monthly Discharges and Annual Characteristics of GRDC Station, Global Runoff Data Cent., Koblenz, Germany. [Available at http://grdc.bafg.de.]
Gorgan, D., V. Bacu, D. Mihon, D. Rodila, K. Abbaspour, and E. Rouholahnejad (2012), Grid based calibration of SWAT hydrological models, *J. Nat. Hazards Earth Syst. Sci.*, *12*, 2411–2423, doi:10.5194/nhess-12-2411-20.
Grizzetti, B., F. Bouraoui, and G. De Marsily (2008), Assessing nitrogen pressures on European surface water, *Global Biogeochem. Cycles*, *22*, GB4023, doi:10.1029/2007GB003085.
Hargreaves, G. L., G. H. Hargreaves, and J. P. Riley (1985), Agricultural benefits for Senegal River Basin, *J. Irrig. Drain. Eng.*, *111*, 113–124.
Haylock, M. R., N. Hofstra, A. M. G. K. Tank, E. J. Klok, P. D. Jones, and M. New (2008), A European daily high-resolution gridded dataset of surface temperature and precipitation, *J. Geophys. Res.*, *113*, D20119, doi:10.1029/2008JD10201.
Holvoet, K., A. van Griensven, P. Seuntjens, and P. A. Vanrolleghem (2005), Sensitivity analysis for hydrology and pesticide supply towards the river in SWAT, *J. Phys. Chem. Earth*, *30*, 518–526, doi:10.1016/j.pce.2005.07.006.
IPCC (2007), Contribution of Working Group II to the fourth assessment report of the IPCC, in *Climate Change 2007: Impacts, Adaptation and Vulnerability*, edited by M. L. Parry, O. F. Canziani, J. P. Palutikof, P. J. van der Linden and C. E. Hanson, pp. 976, Cambridge Univ. Press, Cambridge, U. K.
Jarvis, A., H. I. Reuter, A. Nelson, and E. Guevara (2008), Hole-Filled SRTM for the Globe Version 4, The CGIAR-CSI SRTM 90m Database. [Available at http://srtm.csi.cgiar.org.]
Jensen, M. E. (1968), Water consumption by agricultural plants, in *Water Deficits and Plants Growth*, vol. II, edited by T. T. Kozlowski, pp. 1–22, Academic, N. Y.
Krause, P., D. P. Boyle, and F. Bäse (2005), Comparison of different efficiency criteria for hydrological model assessment, *J. Adv. Geosci.*, *5*, 89–97.
Ludwig, W., E. Dumont, M. Meybeck, and S. Heussner (2009), River discharges of water and nutrients to the Mediterranean and Black Sea: Major drivers for ecosystem changes during past and future decades?, *J. Prog. Oceanogr.*, *80*, 199–217.
Meigh, J. R., A. A. McKenzie, and K. J. Sene (1999), A grid-based approach to water scarcity estimates for eastern and southern Africa, *Water Resour. Manage.*, *13*, 85–115.
Mitchell, T. D., and P. D. Jones (2005), An improved method of constructing a database of monthly climate observations and associated high-resolution grids, *Int. J. Climatol.*, *25*, 693–712, doi:10.1002/joc.1181.
Monfreda, C., N. Ramankutty, and J. A. Foley (2008), Farming the planet: 2. Geographic distribution of crop areas, yields, physiological types, and net primary production in the year 2000, *J. Global Biogeochem. Cycles*, *22*, GB1022, doi:10.1029/2007GB002947.
NASA (2001), Land Processes Distributed Active Archive Center (LP DAAC), ASTER L1B, USGS/Earth Resour. Obs. and Sci. Cent., Sioux Falls, S. D. [Available at http://lpdaac.usgs.gov.]
Neitsch, S. L., J. G. Arnold, J. R. Kiniry, and J. R. Williams (2009), Soil and water assessment tool, theoretical documentation, Version 2009, Agr. Res. Service and Blackland Res. Cent, Temple, Tex.

OSCE/UNECE (2005), *Transboundary Co-operation and Sustainable Management of the Dniester River, Transboundary Diagnostic Study for the Dniester River Basin*, 76 pp., Environ., Housing and Land Manage. Div. U. N. Econ. Comm. for Eur. and Off. of the Coord. of OSCE Econ. and Environ. Activ.

Paleari, S., P. Heinonen, E. Rautalahti-Miettinen, and D. Daler (2005), Transboundary Waters in the Black Sea-Danube Region; Legal and Financial Implications, 53 pp., Univ. of Kalmar, Kalmar, Sweden. [Available at http://www.unep.org/dewa/giwa/areas/reports/r22/giwa_transboundary_waters_in_blacksea.pdf.]

Portmann, F. T., S. Siebert, and P. Döll (2010), MIRCA2000 Global monthly irrigated and rainfed crop areas around the year 2000: A new high resolution data set for agricultural and hydrological modeling, *Global Biogeochem. Cycles*, *24*, GB1011, doi:10.1029/2008GB003435.

Ritchie, J. T. (1972), Model for predicting evaporation from a row crop with incomplete cover, *Water Resour. Res.*, *8*, 1204–1213.

Rouholahnejad, E., K. C. Abbaspour, M. Vejdani, R. Srinivasan, R. Schulin, and A. Lehmann (2012), A parallelization framework for calibration of hydrological models, *J. Environ. Modell. Software*, *31*, 28–36, doi:10.1016/j.envsoft.2011.12.001.

Sommerwerk, N., C. Baumgartner, J. Bloesch, T. Hein, A. Ostojić, M. Paunović, M. Schneider-Jacoby, R. Siber, and K. Tockner (2009), The Danube River Basin, in *Rivers of Europe*, edited by K. Tockner, U. Uehlinger, and C. T. Robinson, chap. 3, pp. 59–112, Academic Press, Burlington, Mass.

Stanners, D., and P. Bourdeau (1995), *Europe's Environment: The Dobris Assessment - An Overview*, Eur. Environ. Agency Task Force, Eur. Environ. Agency, Copenhagen.

Sukhodolov, A. N., N. S. Loboda, V. M. Katolikov, N. A. Arnaut, V. V. Bekh, M. A. Usatii, L. A. Kudersky, and B. G. Skakalsky (2009), Western Steppic Rivers, in *Rivers of Europe*, edited by K. Tockner, U. Uehlinger, and C. T. Robinson, chap. 13, pp. 497–523, Elsevier, doi:10.1016/B978-0-12-369449-2.00013-8.

Tockner, K., U. Uehlinger, and C. T. Robinson (2009), *Rivers of Europe*, Academic, Elsevier.

United Nations Environment Program (UNEP) (2006), Africa Environment Outlook 2: Our environment, our wealth, Div. of Early Warning and Assess., Nairobi, Kenya.

U. S. Geological Survey (USGS) (2008), Global Land Use Land Cover Characterization (GLCC) Database, Reston, Va. [Available at http://edc2.usgs.gov/glcc/globdoc2_0.php.]

Wang, X., X. He, J. R. Williams, R. C. Izaurralde, and J. D. Atwood (2005), Sensitivity and uncertainty analyses of crop yields and soil organic carbon simulated with EPIC, *Am. Soc. Agric. Eng.*, *48*, 1041–1054.

Water Agenda 21 (2011), *Watershed Management. Guiding Principles for Integrated Management of Water in Switzerland*, 20 pp., Swiss Federal Office for the Environment (FOEN), Swiss Federal Office of Energy (FOE), Swiss Federal Office of Agriculture (FOAG), Swiss Federal Office for Spatial Development (ARE), Bern.

Weedon, G. P., S. Gomes, P. Viterbo, W. J. Shuttleworth, E. Blyth, H. Österle, J. C. Adam, N. Bellouin, O. Bouche, and M. Best (2011), Creation of the WATCH forcing data and its use to assess global and regional reference crop evaporation over land during the twentieth century, *J. Hydrometeorol.*, *12*, 823–848.

Wissenschaftlicher Beirat Globale Umweltveränderung (WBGU) (2007), *World in Transition: Climate Change as Security Risk* [in German], Springer, Berlin.

Wolfram, M., and H. Bach (2009), PROMET—Large scale distributed hydrological modelling to study the impact of climate change on the water flows of mountain watersheds, *J. Hydrol.*, *376*(3–4), 362–377, doi:10.1016/j.jhydrol.2009.07.046.

Yang, J., P. Reichert, K. C. Abbaspour, J. Xia, and H. Yang (2008), Comparing uncertainty analysis techniques for a SWAT application to Chaohe Basin in China, *J. Hydrol.*, *358*, 1–23, doi:10.1016/j.jhydrol.2008.05.012.

Zessner, M., and S. Lindtner (2005), Estimations of municipal point source pollution in the context of river basin management, *J. Water Sci. Technol.*, *52*(9), 175–182.

Erratum

In the originally published version of this article, equation (2) was incorrectly typeset. This error has been corrected and this version may be considered the authoritative version of record.